Model reduction of rigid-body molecular dynamics via generalized multipole potentials

Paul N. Patrone, Andrew Dienstfrey, and G. B. McFadden
National Institute of Standards and Technology
100 Bureau Drive, Gaithersburg MD, 20899 USA
(Dated: September 26, 2019)

Motivated by the challenges of uncertainty quantification (UQ) for coarse-grained (CG) molecular dynamics (MD), we investigate the role of perturbation theory in model reduction of classical systems. In particular, we consider the task of coarse-graining rigid-bodies in the context of generalized multipole potentials that have controllable levels of accuracy relative to their atomistic counterparts. We show how the multipole framework yields a hierarchy of models that systematically connects a CG "point-molecule" approximation to the exact dynamics. We use these results to understand when and how the CG models fail to describe atomistic dynamics at the trajectory level and develop asymptotic error estimates for approximate molecular potential energies. Implications for other model-reduction strageties are also discussed. Key findings of this work are that: (i) omitting rotational energy introduces significant error when coarse-graining; and (ii) attention to symmetry can improve accuracy of "point-molecule" approximations. Analytical derivations and numerical results support these conclusions. Relevance to non-rigid bodies is also discussed.

I. INTRODUCTION

Over the past decade, several "bottom-up" approaches to coarse-graining have been proposed as a way to overcome the time- and length-scale limitations of molecular dynamics (MD) [1–15]. However, many of these methods require calibration of the coarse-grained (CG) potentials via costly atomistic simulations. Moreover, the resulting models are known to suffer from *representability* and *transferability* problems in which (i) the definitions of CG observables differ from their atomistic counterparts, and (ii) observables and/or force-fields have non-trivial state-dependence [16–22]. Such problems have made it impossible to construct *a priori* uncertainty estimates for CG predictions because the accuracy (and thus usefulness) of every model must be determined individually at each state-point as part of the calibration. Given that this exercise renders the model-reduction process as expensive as the computations it is meant to replace, coarse-graining has remained a limited tool for materials science.

Fundamentally, the aforementioned issues can be traced to the fact that traditional bottom-up CG methods remove degrees-of-freedom (DOF) in an *ad hoc* manner.[1] In such cases, the CG representation cannot be linked to its atomistic counterpart through a systematic theory controlling the accuracy of the approximation. As a result, important physical processes are eliminated in a way that (i) is inconsistent with the definition of physical observables, and (ii) can only be quantified (and corrected) through comparison with all-atom simulations. Motivated in part by cluster-expansions, this "missing physics" has often been attributed to many-body interactions, and several works have explored the impact of including such effects in CG models [23–25]. Nonetheless, we feel that a deeper *analytical* understanding of how to link atomistic and CG systems through perturbation theory is necessary for enabling more useful uncertainty quantification (UQ).

As a first step in addressing this problem, we consider a new, generalized multipole strategy applied to force-fields of rigid bodies. We take advantage of the well-known fact that the *kinetics* of any such particle can be defined entirely in terms of its center-of-mass and orientation, $\boldsymbol{\chi}$ and a rotation matrix $\boldsymbol{\Theta}$ respectively. Critically, we extend this observation to *dynamics* by showing that the interaction potential between molecules j and j' is also *exactly* expressed in terms of these coordinates, $U_{j,j'} = U(\boldsymbol{\chi}_j, \boldsymbol{\Theta}_j, \boldsymbol{\chi}_{j'}, \boldsymbol{\Theta}_{j'})$. Furthermore, under the assumption that the (constant) interatomic spacings are small relative to the characteristic distance between molecules, the expression for U involves small parameters. Recasting U in terms of a power series then yields a hierarchy of models having controllable accuracy based on truncation order. Importantly, we demonstrate that this hierarchy connects a "point-molecule" CG representation (i.e. in terms of only $\boldsymbol{\chi}$) to its atomistic counterpart [26].[2]

A key objective of this work is to provide an alternate interpretation of bottom-up coarse-graining as a task in

[1] While the coordinate reduction is *ad hoc*, the task of computing the CG force-field is often done systematically via approaches based on structure-matching, force-matching, and/or relative entropy arguments. See Refs. [1–15].

[2] For clarity, we distinguish the concepts of reduced-order modeling and coarse-graining. We treat the former as the more general task of decreasing complexity of a model. In our case, it refers to the fact that $U_{j,j'}$ is approximated to finite (i.e. reduced) order. By coarse-graining, we mean the specific task of eliminating degrees of freedom. We acknowledge, however, that the phrase "coarse-graining in interaction space" has also been used to describe the task of approximating interaction potentials, although we avoid such conventions here.

coordinate *decoupling*, as opposed to coordinate *reduction*. In many contexts, it has been tempting to adopt the latter perspective, since computational efficiency is gained by considering fewer DOF. But, as we show, the benefits may be greater if the reduced DOF are not actually eliminated, but rather decoupled in such a way that they can be modeled analytically. This approach addresses the fundamental motivation for computational approaches (i.e. intractable equations of motion) while preserving more of the all-atom physics. Moreover, it facilitates the development of analytical tools to connect atomistic and CG representations in a way that reveals missing physical processes in the latter. For example, we invoke this perspective to show how omission of rotational energy contributes to errors in our CG models and suggest "zeroth-order" corrections that might improve CG predictions. More generally, our method falls under the category of coarse-graining in interaction space, and we refer the reader to Ref. [26] for connections to other techniques that adopt similar perspectives.

Despite these benefits, our approach has inherent limitations. For one, multipole expansions converge under far-field conditions, i.e. when the characteristic molecular size is small relative to the intermolecular separation. In dense systems this condition may be occasionally, and dynamically, violated. Thus, simulation of dense molecular systems would require reversion to the all-atom interaction for any pair of molecules that are "too close". Moreover, only the limiting case of a point-molecule entails actually reducing degrees of freedom by decoupling $\boldsymbol{\Theta}$ and its associated angular momenta from linear translational motion. However, a key benefit of our approach is that uncertainties associated with these approximations can be established *analytically* in certain cases, which facilitates assessing the quality of a model without expensive atomistic simulations. We show, for example, how the interplay between symmetry and uncertainty can be leveraged *a priori* to render point-molecule approximations accurate at the trajectory level.

It is also important to note that our exposition focuses primarily on uncertainties related to the intermolecular potential energy and the corresponding effects on convergence of coarse-grained trajectories. While predicting the thermodynamic properties of many-body systems is often the primary goal of CG modeling, such quantities are nonetheless extracted from dynamics. Thus, we believe that our initial attempts to understand the limitations of coarse-graining should focus on properties that are actually computed by the simulations. Moreover, such considerations may become important as modelers attempt to extract material properties from non-equilibrium simulations, e.g. diffusion coefficients from velocity autocorrelation functions [27]. We leave consideration of UQ for many-body systems for future work. Finally, this manuscript does not address issues related to the broader concept of UQ, i.e. the process of assessing and building confidence in a simulation. This task involves many additional tasks beyond our scope, such as validation against experiments and determining the quality and usefulness of data. See Refs. [28–35] and the references therein for more information.

A key difficulty of this work is the (to the best of our knowledge) lack of readily-available software packages that can handle the generic class of force-fields we consider. In particular, multipole-based evaluation of potential, force, and torque fields involve contractions of tensors of increasing order, which are not standard in many MD codes. Moreover, discretization of the rigid-body equations require care to preserve the symplectic structure of the system. Indeed, development of computational methods for such systems is an active area of research in the community, with many papers being published in the last few years [36–39]. To maintain strict control over the approximations, we therefore develop custom codes to perform all of our simulations. As these have not been fully optimized, we do not make claims on computational efficiency of our formalism. However, we do discuss preliminary results suggesting decreased runtimes relative to full atom dynamics and discuss further routes for improving efficiency. Detailed analysis of these issues is beyond the scope of this work and is reserved for a future manuscript.

We note that a comparable multipole strategy has been developed for rigid "blobs," i.e. in Ref. 40. Our approach is distinct from this earlier work in several regards. First, the authors of Ref. 40 viewed coarse-graining as a task in "regrouping [rigid] blobs at a finer scale into coarser blobs in the next level up." Thus, the coordinates $\boldsymbol{\chi}$ and (their equivalent of) $\boldsymbol{\Theta}$ do not represent intrinsic or "natural" CG variables of the system, but rather amount to a modeling choice associated with a user-determined coordinate reduction scheme. As a result, $\boldsymbol{\Theta}$ does not play the same role in their analysis as it does in ours [see, e.g. our Eq. (3)]. Second, their focus was largely on statistical properties of many-body simulations, whereas we primarily deal with two-body simulations and trajectory-level properties. Third, our main objective is to develop analytical methods for understanding when and how coarse-graining is accurate or not. Thus our main emphasis is on using generalized multipole approximations to understand the assumptions inherent in coarse-graining.

The rest of this manuscript is organized as follows. Section II reviews the formulation of rigid-body mechanics and equations of motion expressed in terms of $\boldsymbol{\chi}$ and $\boldsymbol{\Theta}$. Section III derives the multipole approximations to the potential, force, and torque. Section IV confirms the analysis by comparison with numerical experiments. We conclude with further discussion and open problems.

II. RIGID-BODY DYNAMICS

Our approach to rigid-body dynamics is adapted from Leimkuhler et al. [41, 42]. Concerning notation, we index components of tensors with lowercase Greek letters, while lowercase Roman letters index particles. Within

tensor formulas we use the Einstein summation convention in which repeated indices are summed over all of their admissible values.

A. Mathematical description of rigid bodies and its connection to coarse-graining

It is useful to review the mathematical characterization of rigid bodies. See also Refs. [41, 43] for related treatments. We consider a molecule composed of P point-particles indexed by k and having mass m_k. By virtue of the rigid-body constraints, the positions $\mathbf{x}_k$ of these particles are fixed relative to one another, so that we may write

$$\mathbf{x}_k = \boldsymbol{\chi} + \mathbf{d}_k, \tag{1}$$

where

$$\boldsymbol{\chi} = M^{-1} \sum_k m_k \mathbf{x}_k \tag{2}$$

is the center of mass, $M = \sum_k m_k$ is the total mass, and $\mathbf{d}_k$ is the position of the kth particle relative to a coordinate system whose origin is $\boldsymbol{\chi}$. We further specify that the axes of this coordinate system are parallel to a fixed laboratory reference frame, so that the $\mathbf{d}_k$ depend on the orientation of the molecule.

We also define a body-frame coordinate system that is fixed to the molecule. In this reference frame, the positions $\boldsymbol{\delta}_k$ of the atoms are constant. The two coordinate systems are connected by a rotation matrix $\boldsymbol{\Theta}$ such that $\mathbf{d}_k = \boldsymbol{\Theta}\boldsymbol{\delta}_k$, where we adopt the convention that all vectors correspond to column vectors. We can therefore express the position of all atoms in the molecule as

$$\mathbf{x}_k = \boldsymbol{\chi} + \boldsymbol{\Theta}\boldsymbol{\delta}_k. \tag{3}$$

Note that the center-of-mass and rotation matrix can be considered as the sole degrees of freedom for the rigid-body molecule. Since the $\boldsymbol{\delta}_k$ are constant, Eq. (3) defines the atomic positions $\mathbf{x}_k$ in terms of fewer variables. The superficial reduction in degrees of freedom[3] — from $\{\mathbf{x}_k,\ k = 1, \ldots, P\}$ to $\{\boldsymbol{\chi}, \boldsymbol{\Theta}\}$ — parallels coarse-graining via the collapse of a molecule onto a point particle (with orientation). This observation plays a central role in the discussion that follows.

Finally, several tensors are helpful to express rigid-body dynamics and compressed representations of intermolecular potentials. These tensors are defined as sums over components of the atomic position vectors, $\boldsymbol{\delta}_k$. We define them here, and reserve discussion of their use until the next section.

[3] For N atoms in a molecule, the number of degrees of freedom is $3N$ less the number of constraints. We have not actually reduced the dimensionality of the system by expressing it in terms of $\boldsymbol{\chi}$ and $\boldsymbol{\Theta}$, since these coordinates implicitly encode the constraints.

Two mass-weighted second-order tensors are convenient for expressing rigid body motion,

$$\boldsymbol{\mathcal{M}} = \sum_k m_k \boldsymbol{\delta}_k \boldsymbol{\delta}_k^{\mathrm{T}} \tag{4}$$

$$\boldsymbol{\mathcal{I}} = \sum_k m_k \left[(\boldsymbol{\delta}_k^{\mathrm{T}} \boldsymbol{\delta}_k)\mathbb{I} - \boldsymbol{\delta}_k \boldsymbol{\delta}_k^{\mathrm{T}} \right], \tag{5}$$

where $\mathbb{I}$ is the identity tensor, and $\boldsymbol{\mathcal{I}}$ is the moment of inertia tensor. The notation $\boldsymbol{\delta}_k \boldsymbol{\delta}_k^{\mathrm{T}}$ denotes a dyadic (or outer) product, so that we may identify $\boldsymbol{\mathcal{M}}$ and $\boldsymbol{\mathcal{I}}$ with matrices. From equations (4) and (5) it is clear that $\boldsymbol{\mathcal{M}}$ and $\boldsymbol{\mathcal{I}}$ are symmetric, and furthermore they commute. Thus, the expressing them in terms of the principal axes of rotation diagonalizes both. We use these axes to define the body-frame coordinate system. In this way the origin and orientation of the molecular body-frame are completely specified.[4]

In addition to the mass-weighted tensors $\boldsymbol{\mathcal{M}}$ and $\boldsymbol{\mathcal{I}}$ needed for dynamics, we also consider *geometric* moments of the rigid bodies. These massless analogs of Eqs. (4) and (5) are key for developing a generalized multipole theory for the intermolecular potential. We define

$$\boldsymbol{\mathcal{C}} = \sum_k \boldsymbol{\delta}_k \tag{6}$$

$$\boldsymbol{\mathcal{K}}^{(2)} = \boldsymbol{\mathcal{K}} = \sum_k \boldsymbol{\delta}_k \boldsymbol{\delta}_k^{\mathrm{T}}. \tag{7}$$

We will refer to $\boldsymbol{\mathcal{C}}$ as the centroid. In tensor notation these give rise to the natural nth-order generalization

$$\mathcal{C}_\alpha = \sum_k \delta_{\alpha,k} \tag{8}$$

$$\mathcal{K}^{(2)}_{\alpha,\beta} = \mathcal{K}_{\alpha,\beta} = \sum_k \delta_{\alpha,k}\delta_{\beta,k} \tag{9}$$

$$\mathcal{K}^{(n)}_{\alpha,\beta,\ldots,\gamma} = \sum_k \delta_{\alpha,k}\delta_{\beta,k}\ldots\delta_{\gamma,k}. \tag{10}$$

Note that for molecules consisting of single atom-types, i.e., $m_k \equiv m$, then $\boldsymbol{\mathcal{C}} = \mathbf{0}$, and $\boldsymbol{\mathcal{M}} = m\boldsymbol{\mathcal{K}}$. However, this is not true in general. Moreover, Eqs. (9) and (10) are symmetric under interchange of any two indices, so that the 3^n elements of $\boldsymbol{\mathcal{K}}^{(n)}$ are highly redundant; see also Ref. 40. While we do not pursue compressed representations here, attention to such details are essential for efficient use of multipole methods.

B. Kinetic and potential energies

For definiteness, we consider a system of N identical rigid bodies indexed by j. Each body is composed of

[4] Strictly speaking there are further degrees of freedom related to axis order and/or subspace rotations in the case of degenerate eigenvalues.

P parts indexed by k and having mass m_k. Given the definitions of the previous section, one may show that the kinetic energy of the jth molecule is [41]

$$K_j(\dot{\boldsymbol{\chi}}_j, \dot{\boldsymbol{\Theta}}_j) = \frac{1}{2} M \dot{\boldsymbol{\chi}}_j^2 + \frac{1}{2} \mathrm{Tr}\left[\dot{\boldsymbol{\Theta}}_j \boldsymbol{\mathcal{M}} \dot{\boldsymbol{\Theta}}_j^{\mathrm{T}}\right],$$

where Tr is the trace operator. If u is the interaction potential characterizing forces between the atomic sites of the rigid body, the intermolecular potential with the j'th rigid body is

$$U_{j,j'}(\boldsymbol{\chi}_j, \boldsymbol{\Theta}_j, \boldsymbol{\chi}_{j'}, \boldsymbol{\Theta}_{j'}) = \sum_{k,k'} u\big(\boldsymbol{\chi}_j - \boldsymbol{\chi}_{j'} + \boldsymbol{\Theta}_j \boldsymbol{\delta}_k - \boldsymbol{\Theta}_{j'} \boldsymbol{\delta}_{k'}\big). \quad (11)$$

Although we have assumed that all interaction sites have identical interactions, it is straightforward to extend Eq. (11) to more general cases, i.e. by indexing u with k and k'.

Several comments are in order. By virtue of the fact that the $\boldsymbol{\delta}_k$ are constant, it is clear that the kinetic and potential energies have been expressed solely in terms of the molecular variables $\boldsymbol{\chi}_j$ and $\boldsymbol{\Theta}_j$ and their time derivatives. Despite this reduction, there is no loss of fidelity in that the individual atomic interactions are retained through the P^2 terms that depend on the pairs $\boldsymbol{\delta}_k, \boldsymbol{\delta}_{k'}$. Thus, our reduced description in terms of molecular centers of mass and orientations is exactly equivalent to the fully atomistic representation.

C. Equations of motion and their integration

The Hamiltonian formulation of rigid body motion is a nontrivial subject with a long history. The issue of suitable discretization strategies gives rise to additional complexity. Rather than repeat these arguments here, we summarize our implementation and refer to the literature for details.

1. Comment on Cross-Products

In the theory of 3-dimensional rotations, cross-products are often used to define angular momentum and related concepts. However, matrix multiplication provides a suitable alternative for this operation, especially given our characterization of orientation in terms of $\boldsymbol{\Theta}$. Thus, it is useful to identify those transformations that convert between matrix and vector representations of the cross product. In particular, we define

$$\mathrm{skew}(\boldsymbol{\omega}) = \begin{pmatrix} 0 & -\omega_3 & \omega_2 \\ \omega_3 & 0 & -\omega_1 \\ -\omega_2 & \omega_1 & 0 \end{pmatrix} \quad (12)$$

$$\mathrm{rot}(\mathbf{A}) = \begin{pmatrix} A_{3,2} - A_{2,3} \\ A_{1,3} - A_{3,1} \\ A_{2,1} - A_{1,2} \end{pmatrix} \quad (13)$$

where $\boldsymbol{\omega}$ is a 3-vector, and $\mathbf{A}$ a 3-by-3 matrix. The following cross-product identities follow directly from these definitions

$$\mathrm{skew}(\boldsymbol{\omega})\mathbf{v} = \boldsymbol{\omega} \times \mathbf{v}, \quad (14)$$

$$\mathrm{rot}(\mathbf{v}\boldsymbol{\omega}^{\mathrm{T}}) = \boldsymbol{\omega} \times \mathbf{v} \quad (15)$$

These will be used repeatedly below.

2. Dynamics

In dynamical systems, rigid body constraints can be implicitly enforced by simultaneously evolving the linear and rotational components of motion. The former amounts to computing the usual forces acting on the center of mass, while the latter entails computing the torque field and the corresponding evolution of the inertia tensor.

We begin by restricting attention to molecule j. The potential due to all other molecules is given by

$$U_j = \sum_{j' \neq j} U_{j,j'}(\boldsymbol{\chi}_j, \boldsymbol{\Theta}_j, \boldsymbol{\chi}_{j'}, \boldsymbol{\Theta}_{j'}), \quad (16)$$

where each $U_{j,j'}$ contains summation over the atomic constituents as in (11). For ease of notation we omit the subscript j, keeping in mind that $\boldsymbol{\chi} = \boldsymbol{\chi}_j$ and $\boldsymbol{\Theta} = \boldsymbol{\Theta}_j$.

The expressions for the force and torque on the j-th molecule, are

$$\mathbf{F} = -\nabla_{\boldsymbol{\chi}} U \quad (17)$$

$$\mathbf{T} = \sum_k \mathbf{d}_k \times \mathbf{F}_k = -\mathrm{rot}\left(\nabla_{\boldsymbol{\Theta}} U \cdot \boldsymbol{\Theta}^{\mathrm{T}}\right) \quad (18)$$

where the gradient with respect to the matrix variable $\boldsymbol{\Theta}$ is defined element-wise as

$$\left(\nabla_{\boldsymbol{\Theta}} U\right)_{\mu,\nu} = \frac{\partial U}{\partial \theta_{\mu,\nu}} \quad (19)$$

The expression for the force acting on the center of mass is standard. The torque computation may be less familiar but, nevertheless, has been derived in several places see [41, 44]. For completeness we include a derivation in the appendix.

We recall the definitions of linear and angular momentum with respect to the center-of-mass:

$$\mathbf{p} = M\dot{\boldsymbol{\chi}} \quad (20)$$

$$\mathbf{L} = \sum_k m_k \mathbf{d}_k \times \dot{\mathbf{d}}_k. \quad (21)$$

For the purpose of writing equations in the body frame we define

$$\boldsymbol{\pi} = \boldsymbol{\Theta}^{\mathrm{T}} \mathbf{L} \quad (22)$$

$$\boldsymbol{\tau} = \boldsymbol{\Theta}^{\mathrm{T}} \mathbf{T} \quad (23)$$

Next, differentiation of the constraint that $\boldsymbol{\Theta}$ is orthogonal ($\boldsymbol{\Theta}\boldsymbol{\Theta}^{\mathrm{T}} = \mathbb{I}$) reveals that the logarithmic derivative $\boldsymbol{\Theta}^{\mathrm{T}}\dot{\boldsymbol{\Theta}}$ is skew symmetric. Following convention we identify the angular velocity vector as

$$\boldsymbol{\Theta}^{\mathrm{T}}\dot{\boldsymbol{\Theta}} = \mathrm{skew}(\boldsymbol{\omega}) \tag{24}$$

Finally, the rigid-body dynamics in the body frame are

$$\left\{\begin{array}{rcl} \dot{\mathbf{p}} &=& \mathbf{F} \\ \dot{\boldsymbol{\chi}} &=& \mathbf{p}/M \end{array}\right. , \quad \left\{\begin{array}{rcl} \dot{\boldsymbol{\pi}} &=& \boldsymbol{\tau} + \boldsymbol{\pi}\times\left(\boldsymbol{\mathcal{I}}^{-1}\boldsymbol{\pi}\right) \\ \dot{\boldsymbol{\Theta}} &=& \boldsymbol{\Theta}\,\mathrm{skew}\left(\boldsymbol{\mathcal{I}}^{-1}\boldsymbol{\pi}\right) \end{array}\right. \tag{25}$$

Numerical integration of Eqs. (25) can be performed via a variety of algorithms. Following convention of the MD community we choose a splitting method analogous to the Verlet class of algorithms, but developed for rigid bodies; see Ref. 41 and 42 for details.

III. MULTIPOLE COARSE-GRAINING

We now have all of the formal ingredients necessary to construct our hierarchy of reduced-order (RO) models (see footnote 2 for the distinction between CG and RO models). The strategy is to approximate the intermolecular potential Eq. (11) using a generalized multipole expansion. The result is a power series in the parameter $|\boldsymbol{\delta}_k|/|\boldsymbol{\chi}|$. In the next few sections, we first outline these steps in the context of a common power-law example, and then discuss the method more generally. Note, the accuracy of this approximation depends on the order of the expansion in combination with the separation between molecular centers. We expect this approach to be more effective when molecules interact through "far-field" conditions. In the following we examine convergence for few-body systems at a very fine scale of analysis, for example, force as a function of position and trajectories in the phase space of the full atomic system. In future work we will extend these results to standard ensembles, e.g. number-volume-temperature (NVT) and number-pressure-temperature (NPT) ensembles.

A. Intermolecular potentials, forces, and torques

We begin by considering $u = r^{-n}$ for some $n > 0$, which is a workhorse of many interatomic potentials (e.g. electrostatic, van Der Waals, etc.). By Eq. (11) one finds an intermolecular potential of the form

$$\begin{aligned} U_{j,j'} &= \sum_{k,k'} \frac{1}{\left(\chi^2 + 2\boldsymbol{\chi}\cdot\boldsymbol{\Delta}_{k,k'} + \Delta_{k,k'}^2\right)^{n/2}}, \\ \boldsymbol{\chi} &= \boldsymbol{\chi}_j - \boldsymbol{\chi}_{j'} \\ \boldsymbol{\Delta}_{k,k'} &= \boldsymbol{\Theta}_j\boldsymbol{\delta}_k - \boldsymbol{\Theta}_{j'}\boldsymbol{\delta}_{k'} \end{aligned} \tag{26}$$

where the "un-bold" symbols refer to magnitudes, i.e. $\chi = |\boldsymbol{\chi}|$ and $\Delta_{k,k'} = |\boldsymbol{\Delta}_{k,k'}|$.

Using Eqs. (17) and (18), one may show that the corresponding intermolecular force and torque (in the laboratory frame) are

$$\mathbf{F} = n\sum_{k,k'} \frac{\boldsymbol{\chi} + \boldsymbol{\Delta}_{k,k'}}{\left(\chi^2 + 2\boldsymbol{\chi}\cdot\boldsymbol{\Delta}_{k,k'} + \Delta_{k,k'}^2\right)^{n/2+1}} \tag{27}$$

$$\mathbf{T} = n\sum_{k,k'} \frac{(\boldsymbol{\Theta}_j\boldsymbol{\delta}_k)\times(\boldsymbol{\chi} + \boldsymbol{\Delta}_{k,k'})}{\left(\chi^2 + 2\boldsymbol{\chi}\cdot\boldsymbol{\Delta}_{k,k'} + \Delta_{k,k'}^2\right)^{n/2+1}} \tag{28}$$

Given these results, it is trivial to write the intermolecular equivalents of more complicated potentials that are linear combinations of power laws. For example, the atomistic Lennard-Jones potential of the form $u(r) = a/r^{12} - b/r^6$ leads to RO forces and torques that are linear combinations of Eqs. (27) and (28). More generally, we may view Eq. (11) and associated expressions for force and torque, Eqs. (17) and (18) respectively, as *reduced-order operators* that transform an atomistic potential into its intermolecular counterpart. As such, one need only compute the RO analogs of a set of atomistic basis potentials, from which we can construct all mappings from atomistic to RO potentials.

Note that the $\boldsymbol{\chi}'s$ and $\boldsymbol{\Theta}'s$ are the only dynamical variables in equations (27) and (28) as the sets of atomic coordinates $\{\boldsymbol{\delta}_k\}$ and $\{\boldsymbol{\delta}_{k'}\}$ are constant. For well-separated small molecules, i.e. whenever

$$\max_{k,k'}\left\{\frac{|\boldsymbol{\delta}_k|}{|\boldsymbol{\chi}|}, \frac{|\boldsymbol{\delta}_{k'}|}{|\boldsymbol{\chi}|}\right\} \ll 1, \tag{29}$$

we expect that the contributions from the summations over atoms in Eqs. (26)–(28) can be approximated in terms of low-order moments. Physically, the motivating idea is that fine-scale molecular structure is not resolved in the far-field of power-law interactions.

B. Multipole expansions

Define $\phi_1 = 2\hat{\boldsymbol{\chi}}\cdot\boldsymbol{\Delta}_{k,k'}$ (where $\hat{\boldsymbol{\chi}} = \boldsymbol{\chi}/\chi$) and $\phi_2 = \Delta_{k,k'}^2$. Using the generalized binomial expansion, Eq. (26) can be expressed as a series expansion of the form

$$\begin{aligned} U_{j,j'} &= \sum_{k,k'} \frac{1}{\chi^n}\left(1 + \frac{\phi_1}{\chi} + \frac{\phi_2}{\chi^2}\right)^{-n/2} \\ &= \frac{P^2}{\chi^n} + \frac{1}{\chi^n}\sum_{k,k'}\sum_{q=1}^{\infty} \frac{(-1)^q\Gamma\left(\frac{n}{2}+q\right)}{\Gamma\left(\frac{n}{2}\right)q!}\left(\frac{\phi_1}{\chi} + \frac{\phi_2}{\chi^2}\right)^q \end{aligned} \tag{30}$$

where $|\phi_1/\chi + \phi_2/\chi^2| < 1$ follows from assumption (29), and $\Gamma(x)$ is the gamma function.

Several comments are in order. Equation (30) may be rearranged into a power series whose terms go as χ^{-n-q} for $q > 0$, the coefficients of which involve expressions of the form $\phi_1^p\phi_2^{p'}$. Interchanging the order of

summation so that $\sum_{k,k'}\sum_q \to \sum_q \sum_{k,k'}$, it is clear that terms $\sum_{k,k'} \phi_1^p \phi_2^{p'}$ can be expressed as functions that map $\hat{\boldsymbol{\chi}}$, $\boldsymbol{\Theta}_j$ and $\boldsymbol{\Theta}_{j'}$ to scalars. *Critically, these functions can be precomputed by summing over k, k' in order to remove explicit reference to the atomistic coordinates.* In other words, we can rewrite Eq. (30) as

$$U_{j,j'} = \frac{P^2}{\chi^n} + \frac{1}{\chi^n}\sum_{q=1}^{\infty} \frac{\mathcal{U}_q(\hat{\boldsymbol{\chi}}, \boldsymbol{\Theta}_j, \boldsymbol{\Theta}_{j'}, \boldsymbol{\mathcal{K}}^{(1)}, ..., \boldsymbol{\mathcal{K}}^{(q)})}{\chi^q} \quad (31)$$

where the $\mathcal{U}_q$ depend on geometric tensors up to order q. As these tensors are precomputed and fixed for the duration of any simulation, evaluation of $\mathcal{U}_q$ no longer require summations over the atomic coordinates.

To see this last point in more detail, consider the first term in the sum of order $\mathcal{O}(\chi^{-n-1})$. One finds that

$$\begin{aligned}\mathcal{U}_1 &= -\frac{n}{2}\sum_{k,k'} \phi_1 \\ &= -n\hat{\boldsymbol{\chi}}^{\mathrm{T}}\Big(\boldsymbol{\Theta}_j \sum_{k,k'} \boldsymbol{\delta}_k - \boldsymbol{\Theta}_{j'} \sum_{k,k'} \boldsymbol{\delta}_{k'}\Big) \\ &= -nP\hat{\boldsymbol{\chi}}^{\mathrm{T}}(\boldsymbol{\Theta}_j - \boldsymbol{\Theta}_{j'})\boldsymbol{\mathcal{C}} \end{aligned} \quad (32)$$

where $\boldsymbol{\mathcal{C}}$ is the centroid as defined in Eq. (6). Likewise, the second order term is given by

$$\begin{aligned}\mathcal{U}_2 &= \sum_{k,k'} -\frac{n}{2}\phi_2 + \frac{n}{4}\left(\frac{n}{2}+1\right)\phi_1^2 \\ &= -n\left(P\,\mathrm{Tr}(\boldsymbol{\mathcal{K}}) - \boldsymbol{\mathcal{C}}^{\mathrm{T}}\boldsymbol{\Theta}_j^{\mathrm{T}}\boldsymbol{\Theta}_{j'}\boldsymbol{\mathcal{C}}\right) \\ &\quad + n\left(\frac{n}{2}+1\right)\hat{\boldsymbol{\chi}}^{\mathrm{T}}\big(P\boldsymbol{\Theta}_j\boldsymbol{\mathcal{K}}\boldsymbol{\Theta}_j^{\mathrm{T}} + P\boldsymbol{\Theta}_{j'}\boldsymbol{\mathcal{K}}\boldsymbol{\Theta}_{j'}^{\mathrm{T}} \\ &\quad - 2\boldsymbol{\Theta}_j\boldsymbol{\mathcal{C}}\boldsymbol{\mathcal{C}}^{\mathrm{T}}\boldsymbol{\Theta}_{j'}^{\mathrm{T}}\big)\hat{\boldsymbol{\chi}}\,. \end{aligned} \quad (33)$$

While more elaborate than $\mathcal{U}_1$, evaluation of $\mathcal{U}_2$ requires only inner products against the geometric moments of the rigid bodies in place of the P^2 computations in terms of the interatomic distances.

In rounding out this section, we provide a few formulas that complete the multipole description. In particular, applying Eqs. (17) and (18) to the above expansion yields

$$\mathbf{F}_0 = n\frac{P^2\boldsymbol{\chi}}{\chi^{n+2}} \quad (34)$$

$$\mathbf{F}_1 = \frac{(n+2)\boldsymbol{\chi}}{\chi^{n+3}}U_1 + \frac{nP}{\chi^{n+2}}\left[\boldsymbol{\Theta}_j - \boldsymbol{\Theta}_{j'}\right]\boldsymbol{\mathcal{C}} \quad (35)$$

$$\begin{aligned}\mathbf{F}_2 = \frac{(n+4)\boldsymbol{\chi}}{\chi^{n+4}}U_2 &+ \frac{2n\boldsymbol{\chi}}{\chi^{n+4}}\Big[P\,\mathrm{Tr}(\boldsymbol{\mathcal{K}}) - \boldsymbol{\mathcal{C}}^{\mathrm{T}}\boldsymbol{\Theta}_j^{\mathrm{T}}\boldsymbol{\Theta}_{j'}\boldsymbol{\mathcal{C}}\Big] \\ &- \frac{n\,(n+2)}{\chi^{n+4}}\Big[P\boldsymbol{\Theta}_j\boldsymbol{\mathcal{K}}\boldsymbol{\Theta}_j^{\mathrm{T}} + P\boldsymbol{\Theta}_{j'}\boldsymbol{\mathcal{K}}\boldsymbol{\Theta}_{j'}^{\mathrm{T}} \\ &\qquad - 2\boldsymbol{\Theta}_j\boldsymbol{\mathcal{C}}\boldsymbol{\mathcal{C}}^{\mathrm{T}}\boldsymbol{\Theta}_{j'}^{\mathrm{T}}\Big]\boldsymbol{\chi} \end{aligned} \quad (36)$$

and

$$\boldsymbol{\tau}_0 = 0 \quad (37)$$

$$\tau_{1,\alpha} = \frac{nP}{\chi^{n+2}}\boldsymbol{\chi}^{\mathrm{T}}\boldsymbol{\epsilon}_\alpha\boldsymbol{\Theta}_j\boldsymbol{\mathcal{C}} \quad (38)$$

$$\begin{aligned}\tau_{2,\alpha} = &\frac{-n}{\chi^{n+2}}\boldsymbol{\mathcal{C}}^{\mathrm{T}}\boldsymbol{\Theta}_{j'}^{\mathrm{T}}\boldsymbol{\epsilon}_\alpha\boldsymbol{\Theta}_j\boldsymbol{\mathcal{C}} \\ &- \frac{n(n+2)}{\chi^{n+4}}\boldsymbol{\chi}^{\mathrm{T}}\boldsymbol{\epsilon}_\alpha\boldsymbol{\Theta}_j\left[P\boldsymbol{\mathcal{K}}\boldsymbol{\Theta}_j^{\mathrm{T}} - \boldsymbol{\mathcal{C}}\boldsymbol{\mathcal{C}}^{\mathrm{T}}\boldsymbol{\Theta}_{j'}^{\mathrm{T}}\right]\boldsymbol{\chi} \end{aligned} \quad (39)$$

where $\mathbf{F}_q$ and $\boldsymbol{\tau}_q$ are the contributions to the forces and torques arising from U_q, and $\boldsymbol{\epsilon}_\alpha = [\epsilon_{\alpha,\beta,\gamma}]$ is a matrix formed from the β and γ components of the Levi-Civita symbol $\epsilon_{\alpha,\beta,\gamma}$.

Finally, the methods discussed here can be generalized to an arbitrary potential as the expansions in Eq. (31) amount to the Taylor series. Thus, taking $u(r)$ to be a generalized potential that is sufficiently differentiable, we may write

$$U = P^2 u(\boldsymbol{\chi}) + \sum_{q,k,k'} u^{(q)}(\boldsymbol{\chi})\frac{(2\boldsymbol{\chi}\cdot\boldsymbol{\Delta}_{k,k'} + \boldsymbol{\Delta}_{k,k'}^2)^q}{q!}, \quad (40)$$

where $u^{(q)}$ denotes the qth derivative of u with respect to $\boldsymbol{\chi}$. Applying the usual formulas to this series provides the corresponding multipole expansions.

Note that the rotation matrix $\boldsymbol{\Theta}$ does not appear in the leading order term of Eq. (40). Thus, at large enough distances the molecular structure and rotational DOF are entirely decoupled from the center-of-mass motion. Stated differently, truncating the multipole expansion at leading order amounts to an approximation in which the angular momentum of each molecule becomes a constant of motion; see also Eq. (37). While such DOF have not been removed from molecular description, their behavior can be computed analytically. Thus, the leading order model implied by Eq. (40) is equivalent to a CG, point-molecule approximation in terms of only $\boldsymbol{\chi}$.

IV. NUMERICAL RESULTS AND THE ROLE OF SYMMETRY IN COARSE-GRAINING

One our main results is the observation that higher-order multipole corrections yield orientation-dependent potentials, forces, and torques. Thus, the coordinate reduction achieved by keeping only the leading-order behavior imposes significant (i.e. radial) symmetry that may not be physically reasonable. By means of numerical experiments and asymptotic estimates, we highlight the importance of this structure on the accuracy of a RO or CG representation. Our exposition has two main parts.

First, we show that the orientation dependence of the force-field can be significant, even for well separated particles. Computing averages over different sets of arguments, we illustrate that projecting this structure onto a radially symmetric potential yields unexpected behavior

not captured by the leading-order multipole potential. Second, we present two-body collisions between idealized molecules with varying degrees of symmetry. These examples demonstrate the critical role played by angular momentum and show how imposing symmetry on a CG model yields inconsistent trajectory level dynamics.

A. Symmetry and convergence of the multipole expansion

Ostensibly Eq. (11) is a function of the center of mass vectors $\boldsymbol{\chi}_j$, $\boldsymbol{\chi}_{j'}$ and orientation variables $\boldsymbol{\Theta}_j$, $\boldsymbol{\Theta}_{j'}$. But in MD, the most popular class of *atomistic* potentials are *central*, i.e., they depend only on the magnitude of the interparticle separation vector

$$u = u\left(|\boldsymbol{\chi}_j - \boldsymbol{\chi}_{j'} + \boldsymbol{\Theta}_j\boldsymbol{\delta}_k - \boldsymbol{\Theta}_{j'}\boldsymbol{\delta}_{k'}|\right). \tag{41}$$

Without loss of generality, we can factor out one of the rotation matrices to find

$$\boldsymbol{\chi}_j - \boldsymbol{\chi}_{j'} + \boldsymbol{\Theta}_j\boldsymbol{\delta}_k - \boldsymbol{\Theta}_{j'}\boldsymbol{\delta}_{k'} = \boldsymbol{\Theta}_{j'}\left[\tilde{\boldsymbol{\chi}} + \tilde{\boldsymbol{\Theta}}\boldsymbol{\delta}_k - \boldsymbol{\delta}_{k'}\right], \tag{42}$$

where $\tilde{\boldsymbol{\chi}} = \boldsymbol{\Theta}_{j'}^{\mathrm{T}}(\boldsymbol{\chi}_j - \boldsymbol{\chi}_{j'})$ and $\tilde{\boldsymbol{\Theta}} = \boldsymbol{\Theta}_{j'}^{\mathrm{T}}\boldsymbol{\Theta}_j$. Because the magnitude of the separation vector in Eq. (42) is independent of an overall rotation, we immediately recognize that $\tilde{\boldsymbol{\chi}}$ and $\tilde{\boldsymbol{\Theta}}$ can be treated as the only independent quantities in u. It follows that central intermolecular potentials and forces exhibit the symmetries

$$U(\boldsymbol{\chi}_j, \boldsymbol{\Theta}_j, \boldsymbol{\chi}_{j'}, \boldsymbol{\Theta}_{j'}) = \tilde{U}(\tilde{\boldsymbol{\chi}}, \tilde{\boldsymbol{\Theta}}) \tag{43}$$

$$\mathbf{F}(\boldsymbol{\chi}_j, \boldsymbol{\Theta}_j, \boldsymbol{\chi}_{j'}, \boldsymbol{\Theta}_{j'}) = \boldsymbol{\Theta}_j\tilde{\mathbf{F}}(\tilde{\boldsymbol{\chi}}, \tilde{\boldsymbol{\Theta}}) \tag{44}$$

where $\tilde{\mathbf{F}}$ is defined with respect to the gradient of the potential. Thus, it is sufficient to consider intermolecular potentials and forces as functions defined on $\boldsymbol{R}^3 \times \mathrm{SO}(3)$, i.e. a position and orientation.

We introduce an interpretation of these variables that is convenient for this discussion. Identifing the lab-frame with the body-frame of molecule j, the separation vector $\tilde{\boldsymbol{\chi}}$ can be described in spherical coordinates in terms of a radius (distance), longitude, and lattitude. The remaining orientation degrees of freedom are then associated with pitch, yaw, and roll of molecule j', which "orbits" the central molecule. From this vantage point, there are at least two ways to derive a spherically symmetric CG potential (or force-field) from u: either (i) ignore the five rotational degrees of freedom altogether, which amounts to setting $\delta_k = 0$ and keeping only the zeroth order multipole term; or (ii) average over the rotation degrees of freedom.

To better understand the differences between these approximations, we consider a Lennard-Jones 6-12 interatomic potential of the form,

$$u(r) = 4\epsilon\left(\left(\frac{\sigma}{r}\right)^{12} - \left(\frac{\sigma}{r}\right)^{6}\right). \tag{45}$$

We report results in the non-dimensional, Lennard-Jones units. Computationally this amounts to setting ϵ and σ both equal to one. Note that in this case, the potential minimum for atom-atom interactions occurs at $r_{min} = 2^{1/6} \approx 1.122$. This is a natural length scale for consideration of atom-atom interactions.

We consider an idealized system composed of triangular rigid bodies with identical atomic interaction sites located at the vertices; thus $P = 3$. We assume the molecules are isosceles and have different masses at each vertex, so that the center-of-mass does not necessarily coincide with the centroid. In the body-frame, the vertices are located at

$$\boldsymbol{\delta}_1 = ab(1, 0, 0)^{\mathrm{T}} \tag{46a}$$

$$\boldsymbol{\delta}_2 = b(-0.5, \sqrt{3}/2, 0)^{\mathrm{T}} \tag{46b}$$

$$\boldsymbol{\delta}_3 = b(-0.5, -\sqrt{3}/2, 0)^{\mathrm{T}} \tag{46c}$$

where a determines the relative length of the two equal sides to the remaining side of the triangle, and b is an overall scale factor determining the size of the molecule. Note that as $b \to 0$, the molecule reverts to a point-particle. For Lennard-Jones molecular systems the combination of b and σ determines a distance beyond which one can expect that the multipole approximation will be effective, c.f. (29). For the following examples, we set $b = 0.2$ and $a = 4$.

We first note that variation with respect to orientation can be significant. As an example we place a "target molecule" at the origin of the lab-frame with an arbitrary but fixed orientation.[5] The location of the source molecule is fixed at $\boldsymbol{\chi}_2 = (0, 0, 3)$. We consider the force on the target molecule as function of $\boldsymbol{\Theta}_2$.

Due to molecular asymmetry, the magnitude of this force varies considerably even at this moderately large separation distance. To illustrate this, in figure 1 we show the distribution of $\|\mathbf{F}\| = \|\mathbf{F}_{1,2}\|$ for 10000 orientations $\boldsymbol{\Theta}_2$ drawn at random from the uniform distribution on SO(3). The distribution in $\|\mathbf{F}_{1,2}\|$ is highly asymmetric and the range is approximately twice the average. For comparison, the distributions are shown when evaluating these same forces using multipole approximations up to order 2. Notice that the zeroth order expansion collapses molecules to points with centrally symmetric interactions. When considered as a function of rotations, the random distribution appears as a delta-function. Clearly this represents a significant structural

[5] For the examples discussed in this section we fixed this orientation to be $\boldsymbol{\Theta}_1 = \mathrm{Euler}(8/11, 16/7, 3)$, where $\mathrm{Euler}(\phi, \theta, \chi)$ is the Euler rotation matrix defined using the zxz-convention [43]. This choice is arbitrary. The intent is to break symmetries that arise when molecular axes are aligned. Alternatively we could have set $\boldsymbol{\Theta}_1$ equal to the identity and fixed the location of the source molecule to be an arbitrary point on a sphere of radius $r = 3$.

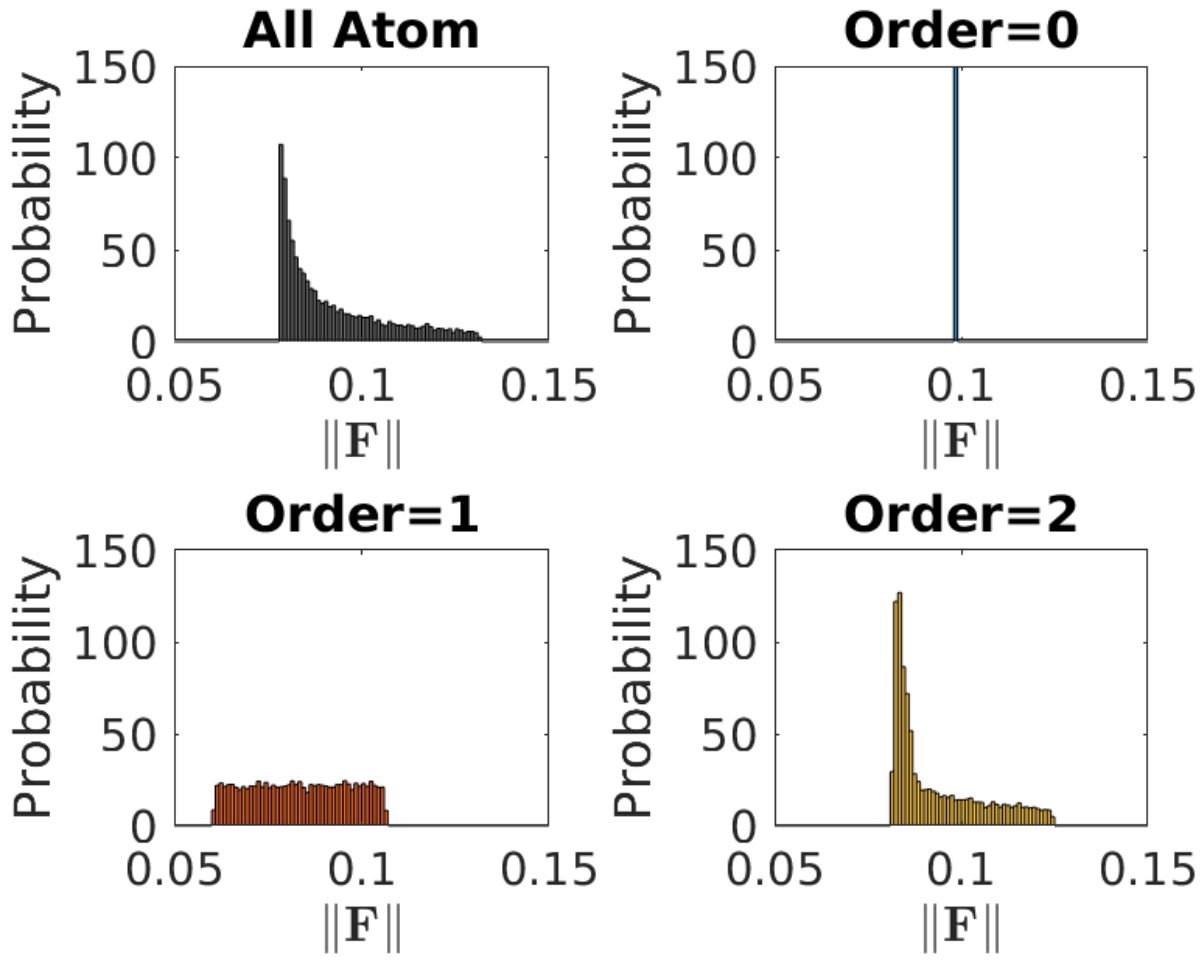

FIG. 1. Probabilities of a given force for a collection of random orientations. *Upper left:* For fixed intermolecular separation, the distribution of $\|\mathbf{F}\|$ as a function of orientation is shown. *Upper right:* The zeroth order multipole expansion is spherically symmetric and cannot capture this variation. Thus the distribution collapses to a delta-function. *Lower left and right:* Higher order multipole expansions converge to the all-atom result.

collapse in comparison to the all-atom computation. Interestingly, including first-order multipole expansions results in an approximately uniform distribution over the same range as the all-atom computation. Finally, the shape of the all-atom force distribution is effectively recovered once second-order terms are included.

As a second example, we average the force over all orientations (i.e. pitch, yaw, and roll) of the source molecule, j'. This entails computing integrals of the form

$$\langle \mathbf{F} \rangle_{SO(3)}(r, \hat{\mathbf{x}}) = \frac{1}{8\pi^2} \int_{SO(3)} \tilde{\mathbf{F}}(r, \hat{\mathbf{x}}, \mathbf{\Theta}) \, \mathrm{d}\Omega(\mathbf{\Theta}) \qquad (47)$$

where r is the radial separation between target and source centers of mass, and $\hat{\mathbf{x}}$ is the corresponding unit vector. Note that Eq. (47) amounts to determining the interaction between a point-particle and a molecule. We approximate the integral by numerical quadrature [45]. Figure 2 shows the magnitude of $\langle \mathbf{F} \rangle_{SO(3)}$ for the triangular molecules as a function of longitude and lattitude. Even after averaging over all orientiations, the force magnitude is a non-trivial function of spherical position. As the zero-th order multipole expansion is a constant on this sphere, it acts only as a shift of this variation. Higher order expansions serve to capture the details more completely.

Finally, we examine the convergence of the multipole represenation as a function of separation distance r. Mathematically we average over all rotational degrees of freedom, orientation and positional, by evaluating the following integral

$$\langle \|\mathbf{F}\| \rangle(r) = \frac{1}{4\pi} \int_{S_2} \|\langle \mathbf{F} \rangle_{SO(3)}(r, \hat{\mathbf{x}})\| \mathrm{d}S(\hat{\mathbf{x}}). \qquad (48)$$

Interestingly, the all-atom forces display a structure that is not visually reminiscent of the Lennard-Jones potential as averaging over the different interaction lengths has

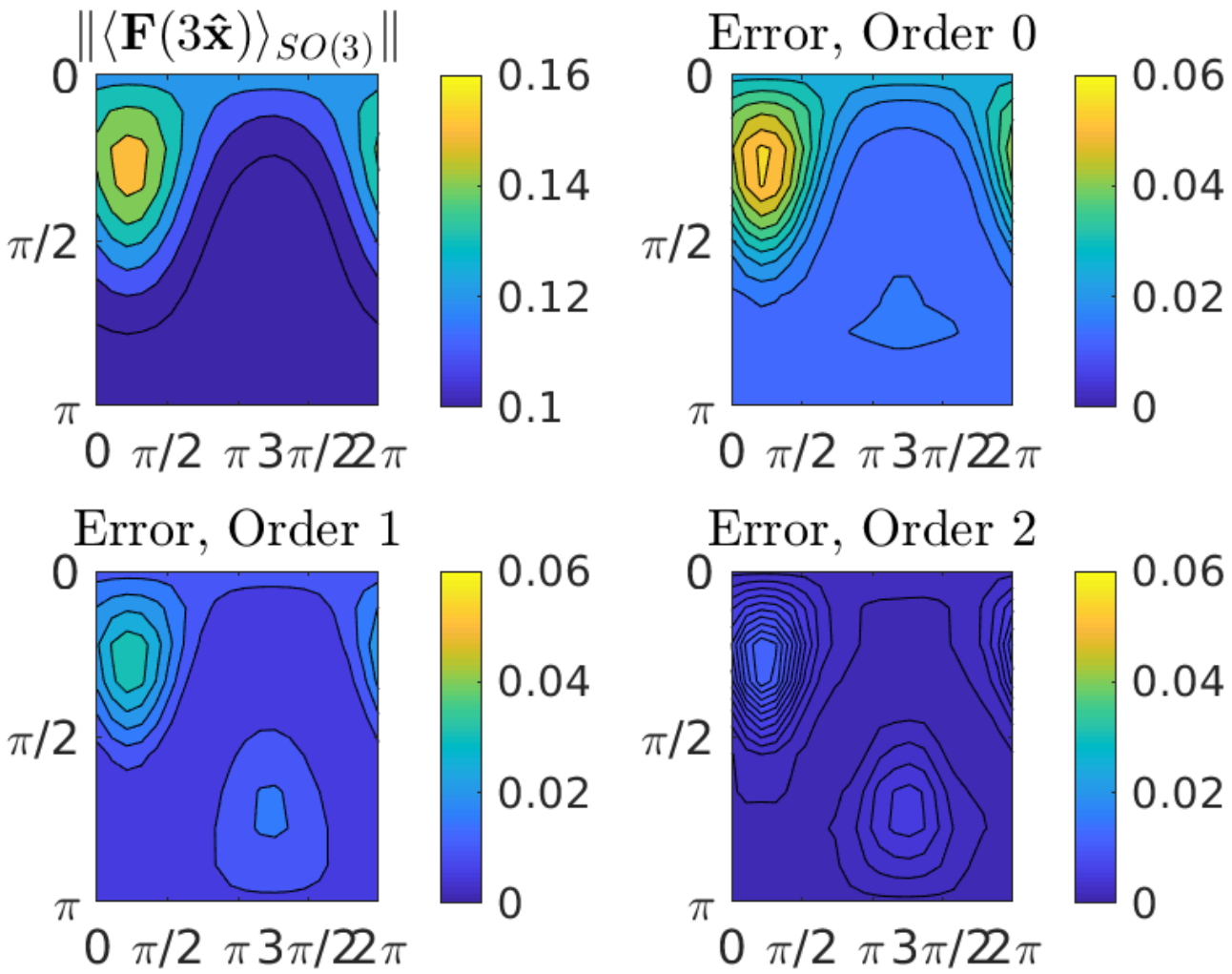

FIG. 2. Force averaged over orientation shown as a function of position. *Upper left:* For fixed intermolecular separation distance $r = 3$, $\|\langle \mathbf{F}\rangle_{SO(3)}\|$ is shown as a function on the sphere parameterized by $3\hat{\mathbf{x}}$, where $\hat{\mathbf{x}}$ is a unit vector between the target and source molecule centers of mass. *Upper right, lower left, lower right:* The multipole evalution converges to the all atom case for increasing order.

the effect of elliminating the clear potential minimum of the single atom-atom potential. In contrast, the zeroth-order approximation *does* arise from a single Lennard-Jones potential, and thereby has relative errors on the order of 20 % or more all the way to $r = 4$. Higher order approximations capture more of the structure of the all-atom potential, as illustrated in the left subplot of the figure. We further discuss the implications of these averaging procedures in Sec. V.

B. Symmetry and Dynamics: Two-Body Collisions

To illustrate the effects of the multipole approximations on dynamics we perform rigid-body simulations of colliding molecules. For convenience, we set $m_1 = m/a$, $m_2 = m_3 = m$ (where m is a mass scale) so that the center of mass is at $\mathbf{r} = 0$ in the body-frame of reference. To advance time, we implement the symplectic algorithm described in Ref. [42], which facilitates evolution of the rotation matrices.

We first consider the case of two-particle dynamics of molecules whose centers-of-mass are on a collision course.

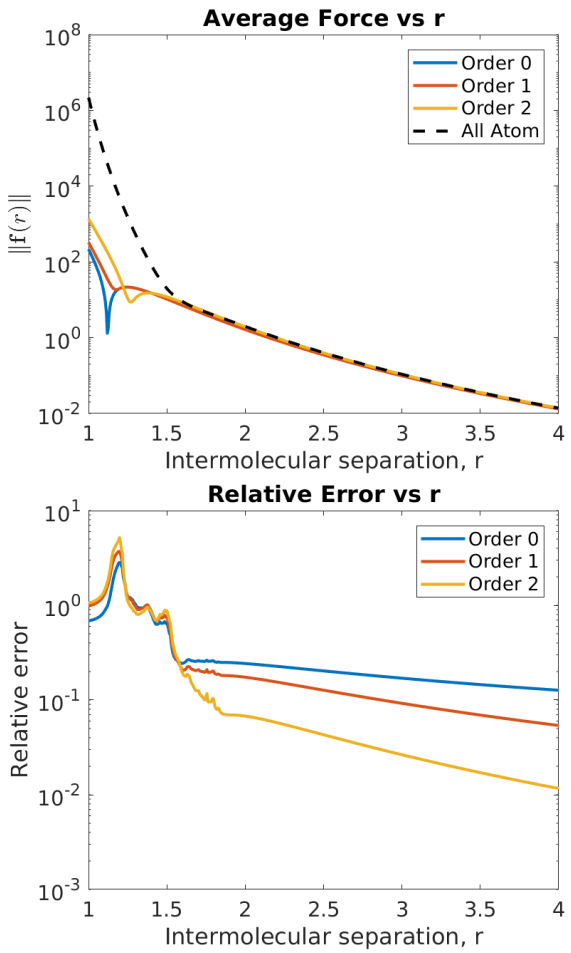

FIG. 3. Force as a function of distance computed by averaging all angular degrees of freedom via Eq. (48). Of note, the all-atom average intermolecular potential bears little resemblance to the Lennard-Jones potential associated with the zeroth-order multipole approximation. The structure of the all-atom force only begins to be captured by higher-order approximations.

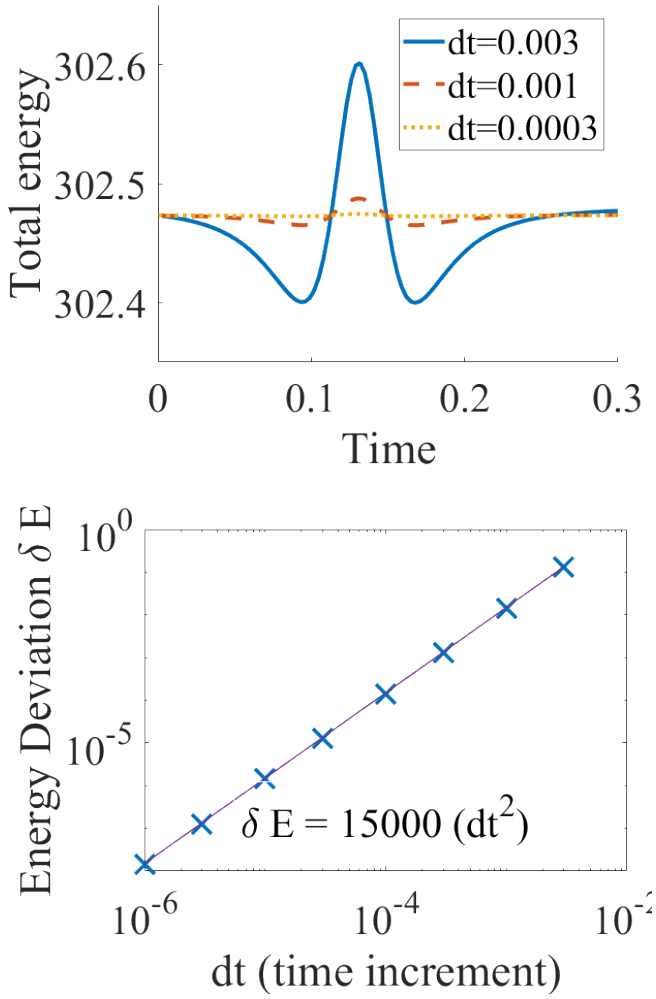

FIG. 4. Energy conservation as a function of timestep for a two-particle collision using an exact intermolecular potential according to Eq. (26) with $u(r) = 300r^{-2}$. *Top*: Total energy as a function of time. Closest approach of the molecules occurs at the maximum value of energy. *Bottom*: Maximum energy deviation $\delta E = \max_t |E(t) - E(0)|$ as a function of time-step $\mathrm{d}t$ (blue $\times$). Note that decreasing the timestep by a decade increases energy conservation by two decades, which is consistent with the a second order numerical integrator. The solid line is the function $\delta E = 15000(dt^2)$.

We prescribe initial conditions as follows:

$$\boldsymbol{\chi}_1 = (-5, 0, -0.25)^{\mathrm{T}} \tag{49a}$$
$$\boldsymbol{\chi}_2 = (5, 0, 0.25)^{\mathrm{T}} \tag{49b}$$
$$\dot{\boldsymbol{\chi}}_1 = (v_1, 0, 0)^{\mathrm{T}} \tag{49c}$$
$$\dot{\boldsymbol{\chi}}_2 = (-v_1, 0, 0)^{\mathrm{T}} \tag{49d}$$
$$\boldsymbol{\omega}_1 = \boldsymbol{\omega}_2 = \mathbf{0} \tag{49e}$$
$$\boldsymbol{\Theta}_1 = \boldsymbol{\Theta}_2 = \mathbf{R}_y(\pi/2)\mathbf{R}_x(\pi/4) \tag{49f}$$
$$a = 4, \quad b = 0.1 \tag{49g}$$
$$m = 0.1 \tag{49h}$$

where $v_1 > 0$ is an adjustable parameter, $\mathbf{R}_\star(\phi)$ is a rotation about the lab-frame $\star$-axis by an angle ϕ, and a and b are as defined in Eqs. (46a)–(46c). We also set the interatomic potential $u(r) = 300r^{-2}$ to be a simple power law repulsion.

As a preliminary assessment of our discretization of the equations-of-motion, we check that energy s conserved to within the time increment $\mathcal{O}(\mathrm{d}t^2)$ as required by the symplectic timestepper. Figure 4 illustrates this conservation for $v_1 = 35$ and $b = 0.2$ using the exact potential at a variety of timestep increments (cf. Fig. 5 for a characteristic trajectory). Quadratic decay of the energy fluctuations is consistent with known results on shadow Hamiltonians and energy conservation for microcanonical molecular dynamics simulations.

Next, we fix $\mathrm{d}t = 10^{-4}$ while varying b (the molecular length-scale) over two decades, from $b = 1$ to $b = 10^{-2}$. Note in particular that as $b \to 0$, the molecules revert to point-particles so that the far-field approximation be-

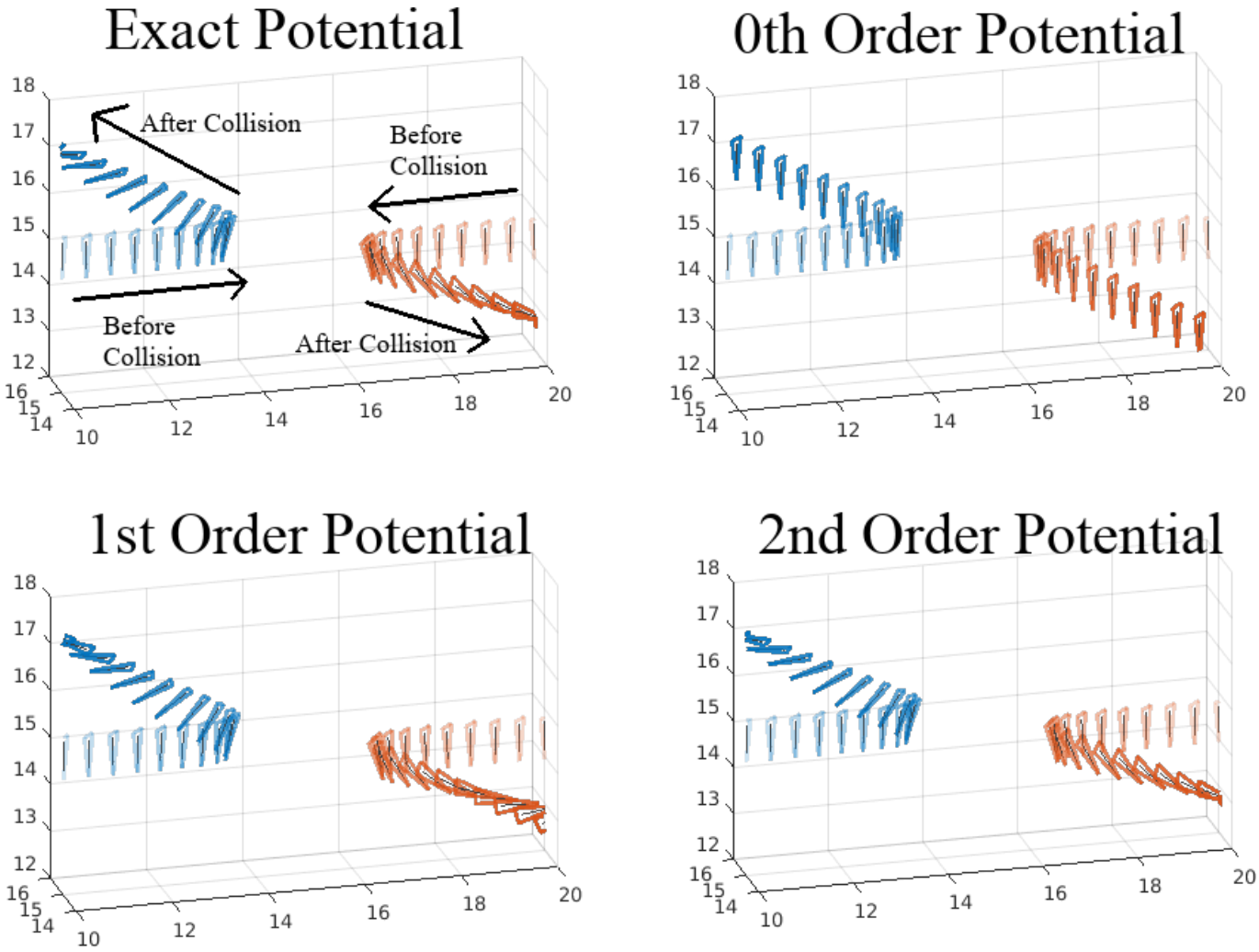

FIG. 5. Example of predictions associated with an exact intermolecular potential and approximations thereof. The four subplots show collision between two triangular particles; the solid black line extends from the center-of-mass to the geometric center. *Top left:* Trajectory computed using the exact potential. Note that the triangular molecules begin rotating after the collision. *Top right:* Trajectory using the zeroth order (radially symmetric) potential. Note that the collision does not induce any rotation in the molecules. *Bottom left:* Trajectory using the first order potential. The molecules over-rotate relative to the top-left sub plot. *Bottom right:* Trajectory computed using the second order.

comes more accurate. Figure 5 shows a sample of characteristic trajectories. Note that the trajectory computed using the exact potential that is poorly captured by the zeroth and first order potentials. To make this observation more quantitative, we also compute convergence in scaled Euclidean norm on the phase-space variables

$$\mathcal{L}(n) = \sum_{j,k} \frac{||\mathbf{x}_{j,k}^{(e)} - \mathbf{x}_{j,k}^{(n)}||^2}{d_\star^2} + \frac{||\mathbf{p}_{j,k}^{(e)} - \mathbf{p}_{j,k}^{(n)}||^2}{p_\star^2} \qquad (50)$$

where the superscripts (e) and (n) refer to the trajectory computing using the exact potential and nth order approximation, $\mathbf{x}_{j,k}$ is the position of the kth atom in the jth molecule, $\mathbf{p}_{j,k}$ is the corresponding momentum, and the normalization factors p_*^2 and d_*^2 are characteristic scales chosen to adimensionalize the measure. [6] Figure 6 shows representative examples of these norms as a function of time for the exact and approximate potentials. As expected, the trajectories computed using approximate potentials converge to their fully atomistic counterparts when $b \to 0$ or when the approximation order increases. Figure 7 shows the corresponding rotational energies as a function of time.

To further understand the impact of low-order approximations, Fig. 8 shows a top-down view trajectories in which the molecular orientation induces signifi-

[6] As an aside, using multipoles up to second order it is possible to express this phase-space norm in terms of $\boldsymbol{\chi}$ and $\boldsymbol{\Theta}$ and their time derivatives.

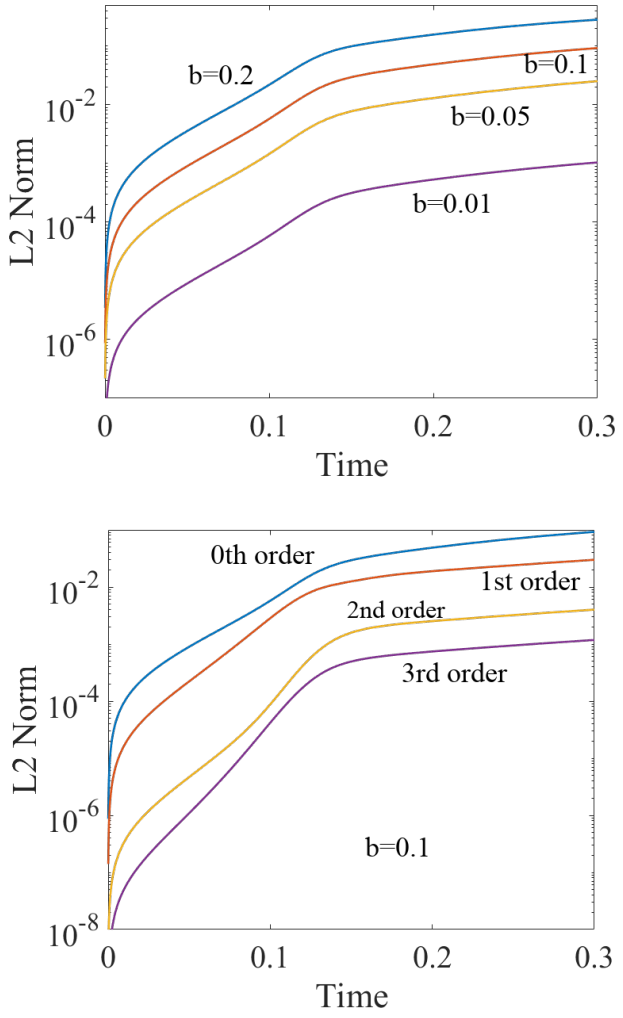

FIG. 6. *Top:* Phase-space norms according to Eq. (50) between trajectories computed using the exact and zeroth order approximation to the intermolecular potential. Note that as the characteristic molecular size goes to zero, the two trajectories increasingly coincide. *Bottom:* The same norms computed for fixed $b = 0.1$ using successively higher-order approximations of the molecular potential. Increasing the approximation order yields better agreement between the coarse-grained and atomistic trajectory.

cant out-of-plane motion after the collision. In particular, we consider the case in which $\mathbf{\Theta}_1 = \mathbf{R}_z(\pi/4)$ and $\mathbf{\Theta}_2 = \mathbf{R}_z(5\pi/4)$, so that both triangles lie in the same plane. Note that the exact and second-order potentials predict deflection in the x-direction after the collision, while the zeroth-order potential does not. Importantly, this discrepancy would hold for any spherically symmetric potential, as can be shown by recourse to symmetry arguments. *Thus, there is no spherically symmetric potential that predicts the correct trajectory to within an arbitrary level of accuracy for a fixed molecular size and minimum separation.* A more general statement to this effect is presented in Sec. V.

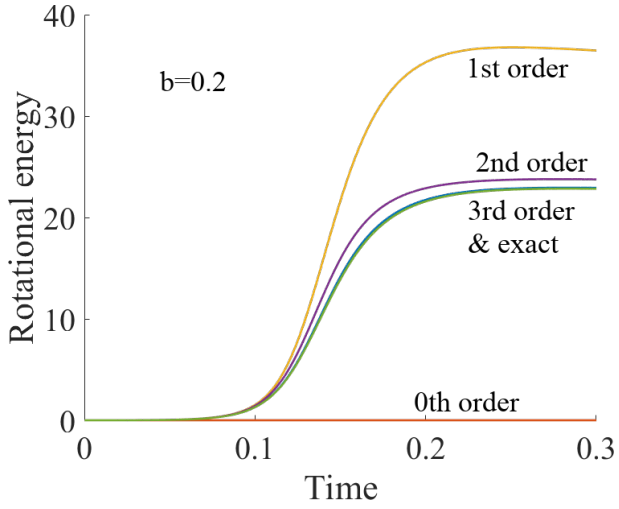

FIG. 7. Rotational energy using the exact and approximate potentials shown in the bottom plot of Fig. 6 (but with $b = 0.2$).

V. DISCUSSION AND CONCLUSIONS

A. Comparison with other coarse-graining methods

Several popular coarse-graining strategies determine intermolecular interactions via potentials of mean force. In short, such approaches specify a mapping from atomic coordinates $\mathbf{r}$ onto a user-defined set of CG coordinates $\mathbf{R}$, $\mathbb{P}(\mathbf{r}) = \mathbf{R}$. The corresponding potential $V_{\mathrm{CG}}(\mathbf{R})$ is defined as the Boltzmann factor satisfying the relation

$$e^{-V_{\mathrm{CG}}(\mathbf{R})/k_BT} = \frac{1}{\mathcal{Z}} \int \mathrm{d}\mathbf{r}\, e^{-V(\mathbf{r})/k_BT} \delta\left(\mathbf{R} - \mathbb{P}(\mathbf{r})\right), \quad (51)$$

where $\mathcal{Z}$ is the partition function, $V(\mathbf{r})$ is the atomistic potential, and the Dirac delta function $\delta\left(\mathbf{R} - \mathbb{P}(\mathbf{r})\right)$ serves to restrict the atomic coordinates to configurations consistent with CG variables $\mathbf{R}$.

Formally, Eq. (51) has the benefit of yielding the exact statistics associated with the CG system. However, the corresponding CG potential depends strongly on the choice of mapping $\mathbb{P}(\mathbf{r})$; there is no *a priori* rule for its construction. Noid and collaborators have worked out the case in which CG variables are linear averages over collections of atoms, i.e., $\mathbb{P}(\mathbf{r})$ may be represented by a matrix in which the sum over each row is one [9]. However in general, coarse-graining strategies based on Eq. (51) must also posit a trial function representation of V_{CG} with parameters that can be fit via optimization against an atomistic simulation. In many cases, objective functions are based on the relative entropy of the approximate and true potentials of mean force, or in some cases, appropriate norms of CG observables.

An interesting feature of this approach is that phase spaces of the atomistic and CG representations are necessarily different, since $\mathbb{P}$ entails a coordinate reduction. As a result, observables that depend on all of the atomistic

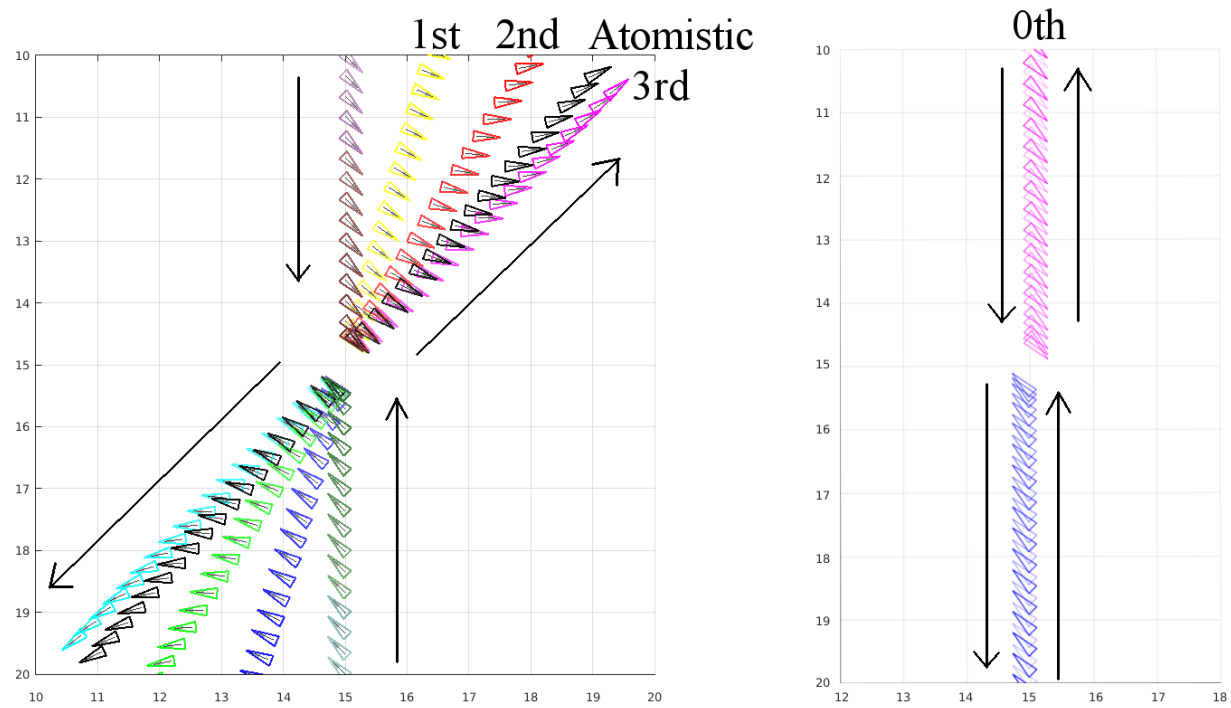

FIG. 8. Top-down view of collision using various approximations to the exact intermolecular potential. *Left:* Comparison of trajectory using the exact potential and corrections to the zeroth order potential. All trajectories follow the same path up to the point of collision and diverge from the atomistic according to their approximation order. The initial conditions are such that the trajectories of the bottom molecule are the same as for the top molecule when rotated by π radians. Note that in all cases, the collision induces rotation and deflection into the x-direction. *Right:* Trajectory computed using the zeroth-order approximate potential. Note the lack of deflection in the x-direction.

coordinates (e.g. the system energy, pressure, temperature, etc.) are not meaningfully defined in terms of the CG simulations. Practically speaking, this means that naive use of the atomistic definitions yields nonsensical results. However, corresponding CG definitions of such observables can be determined *a posteriori* in terms of $\mathbb{P}$ via sampling exercises similar to those used to determine $V_{\rm CG}$. The recognition that this sampling is computationally expensive has been termed the "representability" problem, and the task of finding efficient and/or analytical methods of determining the CG observables remains an open problem [21, 46].[7,8]

While the generalized multipole expansions are more limited in their ability to reduce the complexity of a model, by construction they do not change the measure-space of the reduced-order model. This is because "coarse-graining" occurs through coordinate decoupling; i.e. the degenerate, spherically symmetric potentials allow the angular DOF to evolve independently in a way that can be computed by hand. While the implications of this observation lie beyond the scope of this manuscript, we recognize, for example, that this amounts to replacing Eq. (51) with

$$e^{V_{\rm CG}(\mathbf{X})} \propto \int \mathrm{d}\mathbf{\Pi}\; e^{V_1(\mathbf{X})+V_2(\mathbf{\Pi})} \propto e^{V_1(\mathbf{X})} \tag{52}$$

where $\mathbf{X}$ and $\mathbf{\Pi}$ refer to the collection of generalized position and momentum variables, and their separability is the manifestation of the coordinate decoupling. The extent to which such approximations induce errors in CG predictions remains an open problem. See also Ref. 26 for a related approach that considers the concept of coarse-graining in interaction space.

B. Implications for uncertainty quantification of coarse-graining

For many-body systems, we speculate that it is possible to construct *formal, a priori* uncertainty quantification estimates associated with a given multipole approximation. That is, assuming that the probability

[7] Taking the logarithm of Eq. (51) also reveals that $V_{\rm CG}$ may have non-trivial temperature dependence. This is often called the "transferability" problem, since it means that $V_{\rm CG}$ may need to be determined through sampling at each state-point of interest.

[8] The representability problem has also been understood as an inability to reproduce all atomistic predictions using CG simulations. Reference 21 reconciles this definition with the one we give.

of any given rigid-body microstate is given by $P \propto \exp(-H/k_BT)$ (where H is the Hamiltonian), the difference in an exact and CG observable G can be written as

$$\langle G\rangle_E - \langle G\rangle_A = \int \mathrm{d}\mathbf{X}\mathrm{d}\mathbf{\Pi}\; G(\mathbf{X},\mathbf{\Pi})\;\left[P_E - P_A\right], \quad (53)$$

where the E and A subscripts refer to probabilities associated with the exact and approximate Hamiltonians, and $\mathbf{X}$ and $\mathbf{\Pi}$ have the same meanings as before. Because we have given analytical expressions for the exact and approximate potentials, one can write

$$H_E = H_A + \mathcal{O}\left[\left(\frac{\delta}{\boldsymbol{\chi}_{\min}}\right)^n\right], \quad (54)$$

where the power n corresponds to the first omitted term in the multipole approximation. Here $\boldsymbol{\chi}_{\min}$ is likely a characteristic minimum separation between molecules, which we speculate can be estimated on the basis of analytical, asymptotic expressions for the radial distribution function (RDF) given by Widom [47]. Given this, it may be possible to expand the difference $P_E - P_A$ in powers of $\delta/\boldsymbol{\chi}_{\min}$ and thereby compute estimates of the associated error in the observables. More detailed statements to this effect are open questions that we aim to address in future work.

C. Extensions to inhomogeneous and non-rigid systems

Generalizations to multi-component systems are straightforward. In more detail, the aforementioned derivations only assume a mono-component system insofar as the δ_k are taken to be the same within each molecule. Relaxing this restriction leads to different inertia and geometric moment-tensors for the molecules. Thus, the tensors specific to each molecule in an interaction would appear in each term of the multipole expansion, with the only other modifications coming from the precise form of the atomistic interaction potential. Such details will be addressed in a manuscript under preparation.

We also anticipate that our approach can be modified to address non-rigid systems. In such cases, a new length-scale will emerge, associated with the fluctuations in bond distances. It is likely that such effects are comparable to second-order multipole approximations. Furthermore, we speculate that molecular vibrations can be treated independently in terms of the eigenmodes of the molecule. In such cases, it may be possible to omit certain modes by introducing their average energy into the Hamiltonian.

D. Computational efficiency

Computationally, low-order multipole computations are more efficient than all-atom calculations. However we have not explored in detail the relative efficiency of the potential interactions. The direct atomistic approach requires $O(P^2)$ summations per molecule whereas the multipole expansion captures this geometric distribution once, and replaces the pairwise interactions with tensor contractions. Symmetry inherent in these tensors can be exploited to reduce storage memory requirements, although analysis of these issues is beyond the scope of this work. Nonetheless, we report on preliminary computational observations.

All of the simulation steps are written in Matlab [48].[9] The potential, force, and torque for each fixed pair interaction are computed using a vectorized code for both the all-atom and multipole potentials. Thus, there is no significant looping penalty inherent in the all-atom computation, which effectively does the P^2 atom-atom computations simultaneously. On a 16-core machine, we find that 10^6 force computations using random positions and orientations take roughly 73 seconds for the all-atom computation, 16 seconds for zeroth order, 27 seconds for first order, and 70 seconds for second order. Thus, it appears that within our own code there is a break-even point in terms of computational time around the second-order approximation. We stress, however, that these results are preliminary and do not reflect any attempts to optimize the computations.

Provided that computational gains are limited to first or at most second-order potentials, our generalized multipole method may still be useful in a manner analogous to fast-multipole methods, where approximations are only made for well-separated particles. In this case, it may be fruitful to construct a hybrid potential that uses the exact potential for nearest neighbors and a low-order multipole potential for well separated molecules. It is also important to note that when low-order potentials contain long-range effects that decay as $1/r$, periodic boundary conditions may require the use of lattice summation methods, e.g. in the spirit of Ewald summation [49]. Such approaches may diminish the computational gains associated with coarse-graining, although a detailed study of such issues is beyond our scope.

E. Conclusions, Limitations, and Open Directions

One of the most compelling aspects of coarse-graining is the promise of being able to choose the length-scale associated with the elements of a model. Our work highlights a fundamental question that arises in this context: in so choosing the scale, how does one control the accuracy of a CG model?

---

[9] Certain commercial products are identified in this work in order to specify the computational procedure adequately. Such identification is not intended to imply recommendation or endorsement by the National Institute of Standards and Technology, nor is it intended to imply that the materials or equipment identified are necessarily the best available for the purpose.

As we have shown, it is critical to address this question as an integral part of the coarse-graining task. Otherwise, one risks eliminating relevant physics, or equally problematic, introducing unwanted physics. That being said, there is a natural tension between coarse-graining and accuracy. The latter necessarily entails constraints on the model reduction process, since certain CG representations cannot be reasonable for all problems at all scales. In the context of our multipole approach, this manifests as a restriction that the CG particles correspond (at least approximately) to rigid bodies. As a result, our method can likely only reduce the number of degrees of freedom by at most a factor of ten or so, since large molecules containing, e.g. a few carbon atoms, tend to exhibit significant bond rotation and related motion.

More generally, our work points to the following open questions: (I) when and *how* can physical processes be coarse-grained and still yield a reduced-order model whose accuracy is both reasonable and quantifiable *a priori*; (II) provided this task is possible, under what conditions do all physical observables or only a subset thereof remain accurate; and (III) to what extent can (I) and (II) be addressed analytically for a reasonable class of practical systems?

Many of the past works cited herein provide empirical evidence that there is an optimistic resolution to question (I), but to the best of our knowledge, there is little, if any analytical understanding. Question (II) is more disconcerting in that most CG strategies are known to correctly predict only a few physical quantities. We speculate that *only* those physical properties that do not depend on the omitted or introduced physics can be correctly predicted, save perhaps the use of recalibration steps, which introduce their own uncertainties. Question (III) is perhaps the most difficult, given the complexity of modeling many-body systems in the first place. Here again, we speculate that a deeper understanding of how to analytically treat highly correlated systems may be necessary if progress is to be made.

In this light, our multipole coarse-graining approach is designed to provide a prototypical strategy for addressing all three questions. Specifically, forces associated with the internal structure of a molecule only matter at close range and can be coarse-grained to varying degrees depending on how well far-field conditions hold. Provided this is done self-consistently (in the sense of perturbation theory), all CG observables should have controllable accuracy relative to the atomistic predictions. What is most useful, however, is *how* the coarse-graining is actually achieved: in constrast to methods that modify the molecular structure, we alter the interaction potential. Importantly, these two approaches are not equivalent, since changing structure alters both the free-body motion and interactions in a discontinuous way. In contrast, the multipole approach views coarse-graining as a task decoupling various degrees of freedom (e.g. orientational from translational) in such a way that accuracy can be progressively dialed in. Ultimately we believe that further development of such techniques will be necessary for a complete understanding of the true capabilities and limitations of coarse-graining.

Acknowledgements: The authors thank Yuri Mishin for helpful feedback during preparation of this manuscript.

Appendix A: Derivation of torque

We derive equation (18) expressing the torque on the jth molecule in terms of the gradient with respect to $\mathbf{\Theta}_j$. First, given an arbitrary function $u(\boldsymbol{\chi}+\mathbf{\Theta}\boldsymbol{\delta})$, applying the definition of this gradient given by equation (19), by the chain-rule one finds that

$$\nabla_{\mathbf{\Theta}} u(\boldsymbol{\chi}+\mathbf{\Theta}\boldsymbol{\delta}) = \begin{pmatrix} u_x(\boldsymbol{\chi}+\mathbf{\Theta}\boldsymbol{\delta})\delta_x & u_x(\boldsymbol{\chi}+\mathbf{\Theta}\boldsymbol{\delta})\delta_y & u_x(\boldsymbol{\chi}+\mathbf{\Theta}\boldsymbol{\delta})\delta_z \\ u_y(\boldsymbol{\chi}+\mathbf{\Theta}\boldsymbol{\delta})\delta_x & u_y(\boldsymbol{\chi}+\mathbf{\Theta}\boldsymbol{\delta})\delta_y & u_y(\boldsymbol{\chi}+\mathbf{\Theta}\boldsymbol{\delta})\delta_z \\ u_z(\boldsymbol{\chi}+\mathbf{\Theta}\boldsymbol{\delta})\delta_x & u_z(\boldsymbol{\chi}+\mathbf{\Theta}\boldsymbol{\delta})\delta_y & u_z(\boldsymbol{\chi}+\mathbf{\Theta}\boldsymbol{\delta})\delta_z \end{pmatrix} = \nabla_{\boldsymbol{\chi}} u(\boldsymbol{\chi}+\mathbf{\Theta}\boldsymbol{\delta})\boldsymbol{\delta}^T.$$

Here $u_x(\boldsymbol{\chi}+\mathbf{\Theta}\boldsymbol{\delta})$ is shorthand for evaluation of the partial derivative of $\partial u/\partial x$ at the point $\boldsymbol{\chi}+\mathbf{\Theta}\boldsymbol{\delta}$, and similarly for u_y and u_z.

Next we define the potential field resulting from all atoms on all molecules other than the jth and re-write the sums in equations (16) and (11) in terms of this function

$$\widetilde{U}(\mathbf{r}) = \sum_{j'\neq j}\sum_{k'} u(\mathbf{r}-\mathbf{x}_{k'})$$

$$U_j(\boldsymbol{\chi},\mathbf{\Theta}) = \sum_k \widetilde{U}_j(\boldsymbol{\chi}+\mathbf{\Theta}\boldsymbol{\delta}_k)$$

Finally, recalling the identity (15) we have

$$\begin{aligned}
-\mathrm{rot}\left(\nabla_{\boldsymbol{\Theta}} U_j \cdot \boldsymbol{\Theta}^{\mathrm{T}}\right) &= \sum_k \mathrm{rot}\left(-\nabla_{\boldsymbol{\Theta}} \widetilde{U}\left(\boldsymbol{\chi} + \boldsymbol{\Theta}\boldsymbol{\delta}_k\right) \cdot \boldsymbol{\Theta}^{\mathrm{T}}\right) \\
&= \sum_k \mathrm{rot}\left(\mathbf{F}_k \cdot \mathbf{d}_k^{\mathrm{T}}\right) \\
&= \sum_k \mathbf{d}_k \times \mathbf{F}_k \\
&= \mathbf{T}.
\end{aligned}$$

[1] F. Müller-Plathe, ChemPhysChem **3**, 754 (2002).
[2] D. Reith, M. Putz, and F. Muller-Plathe, Journal of Computational Chemistry **24**, 1624 (2003).
[3] S. Izvekov and G. A. Voth, The Journal of Physical Chemistry B **109**, 2469 (2005).
[4] M. Babadi, R. Everaers, and M. R. Ejtehadi, The Journal of Chemical Physics **124**, 174708 (2006).
[5] J. Zhou, I. F. Thorpe, S. Izvekov, and G. A. Voth, Biophysical Journal **92**, 4289 (2007).
[6] L. Monticelli, S. K. Kandasamy, X. Periole, R. G. Larson, D. P. Tieleman, and S.-J. Marrink, Journal of Chemical Theory and Computation **4**, 819 (2008).
[7] P. Liu, Q. Shi, H. D. III, and G. A. Voth, The Journal of Chemical Physics **129**, 214114 (2008).
[8] M. S. Shell, The Journal of Chemical Physics **129**, 144108 (2008).
[9] W. G. Noid, J.-W. Chu, G. S. Ayton, V. Krishna, S. Izvekov, G. A. Voth, A. Das, and H. C. Andersen, The Journal of Chemical Physics **128**, 244114 (2008).
[10] M. R. Betancourt and S. J. Omovie, The Journal of Chemical Physics **130**, 195103 (2009).
[11] C. Peter and K. Kremer, Soft Matter **5**, 4357 (2009).
[12] H. M. Cho and J.-W. Chu, The Journal of Chemical Physics **131**, 134107 (2009).
[13] A. Lyubartsev, A. Mirzoev, L. Chen, and A. Laaksonen, Faraday Discuss. **144**, 43 (2010).
[14] B. Bayramoglu and R. Faller, Macromolecules **45**, 9205 (2012).
[15] M. G. Saunders and G. A. Voth, Annual Review of Biophysics **42**, 73 (2013).
[16] N. J. H. Dunn, T. T. Foley, and W. G. Noid, Accounts of Chemical Research **49**, 2832 (2016).
[17] A. Louis, J. Phys. Condens. Matter **14**, 9187 (2002).
[18] P. Carbone, H. A. K. Varzaneh, X. Chen, and F. Müller-Plathe, J. Chem. Phys. **128**, 064904 (2008).
[19] K. Farah, A. C. Fogarty, M. C. Boehm, and F. Müller-Plathe, Phys. Chem. Chem. Phys **13**, 2894 (2011).
[20] J. Ghosh and R. Faller, Mol. Simul. **33**, 759 (2007).
[21] J. W. Wagner, J. F. Dama, A. E. P. Durumeric, and G. A. Voth, The Journal of Chemical Physics **145**, 044108 (2016).
[22] P. N. Patrone, T. W. Rosch, and F. R. Phelan Jr., Journal of Chemical Physics **144**, 154101 (2016).
[23] A. Das and H. C. Andersen, The Journal of Chemical Physics **131**, 034102 (2009).
[24] L. Larini, L. Lu, and G. A. Voth, The Journal of Chemical Physics **132**, 164107 (2010).
[25] A. Das and H. C. Andersen, The Journal of Chemical Physics **136**, 194114 (2012).
[26] S. Izvekov, J. M. J. Swanson, and G. A. Voth, The Journal of Physical Chemistry B **112**, 4711 (2008).
[27] T. Gaskell, Journal of Physics C: Solid State Physics **4**, 1466 (1971).
[28] R. Smith, *Uncertainty Quantification: Theory, Implementation, and Applications*, Computational Science and Engineering (SIAM, 2013).
[29] F. Rizzi, R. E. Jones, B. J. Debusschere, and O. M. Knio, The Journal of Chemical Physics **138**, 194105 (2013).
[30] F. Rizzi, R. E. Jones, B. J. Debusschere, and O. M. Knio, The Journal of Chemical Physics **138**, 194104 (2013).
[31] F. Rizzi, H. N. Najm, B. J. Debusschere, K. Sargsyan, M. Salloum, H. Adalsteinsson, and O. M. Knio, Multiscale Modeling & Simulation **10**, 1428 (2012), http://dx.doi.org/10.1137/110853169.
[32] F. Rizzi, H. N. Najm, B. J. Debusschere, K. Sargsyan, M. Salloum, H. Adalsteinsson, and O. M. Knio, Multiscale Modeling & Simulation **10**, 1460 (2012), http://dx.doi.org/10.1137/110853170.
[33] L. C. Jacobson, R. M. Kirby, and V. Molinero, The Journal of Physical Chemistry B **118**, 8190 (2014).
[34] P. Patrone, A. Kearsley, and A. Dienstfrey, "The role of data analysis in uncertainty quantification: case studies for materials modeling," in *2018 AIAA Non-Deterministic Approaches Conference*.
[35] P. N. Patrone and A. Dienstfrey, "Uncertainty quantification for molecular dynamics," in *Reviews in Computational Chemistry, Volume 31* (John Wiley & Sons, Ltd, 2018) Chap. 3, pp. 115–169.
[36] Y. Kajima, M. Hiyama, S. Ogata, R. Kobayashi, and T. Tamura, The Journal of Chemical Physics **136**, 234105 (2012).
[37] R. I. McLachlan, K. Modin, and O. Verdier, Phys. Rev. E **89**, 061301 (2014).
[38] A. Vitalis and R. V. Pappu, The Journal of Chemical Physics **141**, 034105 (2014).
[39] A. J. Silveira and C. R. A. Abreu, The Journal of Chemical Physics **147**, 124104 (2017).
[40] S. D. Chao, J. D. Kress, and A. Redondo, The Journal of Chemical Physics **122**, 234912 (2005).
[41] B. Leimkuhler and C. Matthews, *Molecular Dynamics with Deterministic and Stochastic Numerical Methods* (Springer International Publishing, Switzerland, 2015).
[42] A. Dullweber, B. Leimkuhler, and R. McLachlan, The Journal of Chemical Physics **107**, 5840 (1997).

[43] H. Goldstein, C. Poole, and J. Safko, *Classical Mechanics* (Addison Wesley, 2002).
[44] M. P. Allen and G. Germano, Molecular Physics **104**, 3225 (2006).
[45] M. Graf and D. Potts, Numerical Functional Analysis and Optimization **30**, 665 (2009).
[46] M. E. Johnson, T. Head-Gordon, and A. A. Louis, The Journal of Chemical Physics **126**, 144509 (2007).
[47] B. Widom, The Journal of Chemical Physics **39**, 2808 (1963).
[48] MATLAB, *version 8.1.0 (R2013a)* (The MathWorks Inc., Natick, Massachusetts, 2013).
[49] J. Kolafa and J. W. Perram, Molecular Simulation **9**, 351 (1992).